Journal of Materials Chemistry A

Accepted Manuscript

ROYAL SOCIETY OF CHEMISTRY

www.rsc.org/materialsA

Cite this: DOI: 10.1039/c0xx00000x

ARTICLE

www.rsc.org/xxxxxx

Concave and Duck Web-like Platinum Nanopentagon with Enhanced Electrocatalytic Properties for Formic Acid Oxidation

Jianping Lai,[a,b] Wenxin Niu,[a] Suping Li,[a] Fengxia Wu,[a,b] Rafael Luque,*[a,c] Guobao Xu*[,a]

Received (in XXX, XXX) Xth XXXXXXXXX 20XX, Accepted Xth XXXXXXXXX 20XX

DOI: 10.1039/b000000x

Pt-branched structures featuring concave and duck web-like platinum nanopentagons (CWPNP), with surfaces enclosed by {111} facets, high-energy {110} and {554} facets, multiple twin boundaries, duck-web like edges and inherent anisotropic branches are herein reported. The unique chemisorption properties and reducing capacities of tri-n-propylamine and oleylamine, as well as the inhibition of oxidative etching of the twin defects by the exclusion of chloride ions contribute to the formation of Pt CWPNP. Pt CWPNP exhibited unprecedented electrocatalytic activities, high antipoisoning activity and durability in formic acid oxidation (FOR) in comparison to commercial Pt/C and Pt black, and thus is a promising catalyst for FOR. The excellent FOR performance of Pt CWPNP is attributed to least poisoned {111} facets, active sites by high-energy facets, multiple twin boundaries, duck-web like edges and inherent anisotropic branches composed of 1D nanowires. It is anticipated that this work will offer a new approach to design surface structure-controlled FOR electrocatalysts.

1. Introduction

The direct formic acid fuel cell (DFAFC) is one of the most attractive fuel cells due to the inherent advantages of formic acid as fuel (e.g. safer and easier to store and handle than hydrogen (120 MJ/Kg). Formic acid has also a considerable energy density (1740 W h kg^{-1} or 2086 W h L^{-1}) and a two orders of magnitude lower crossover flux through a Nafion membrane as compared to methanol, thus allowing the utilization of a highly concentrated fuel solution in a DFAFC.[1-28] The development of active anode catalysts for formic acid oxidation reaction (FOR) is therefore an active area of research. Pt is most commonly used electrocatalyst in practical FOR applications (in spite of the higher activity observed for Pd) due to its high tolerance to acidic solutions. FOR can be considered as a structure-sensitive reaction on platinum surfaces. Improving the poisoning resistance, activity and stability of Pt is beneficial for DFAFC eventual commercialization. It is generally accepted that FOR on Pt proceeds by a dual-path mechanism consisting of indirect and direct paths.[11, 13, 19] Direct oxidation produces CO_2 by dehydrogenation (via different intermediates), while indirect oxidation involves a non-Faradaic dehydration of formic acid to form poisoning CO_{ads} and subsequent oxidation of CO_{ads} to CO_2. Generally speaking, Pt (111) facets are the direct pathway and least poisoned surface for FOR.[29-32] Pt high-energy facets have higher FOR activity with respect to low-index facets due to the fact that high-energy facets exhibit high density of atomic steps, edges and kinks on their surface and these active sites are especially important for breaking chemical bonds in catalytic reactions.[33-37] In addition, Pt twinned nanoparticles comparatively show higher catalytic activities to those of single crystal nanoparticles as twinned defects entail considerable surface-active sites on the surface of nanoparticles with a significant facilitate the oxidation process.[38, 39] The catalytic stability of FOR is also structure-sensitive on nanoparticle surfaces. One-dimensional (1 D) nanostructures including nanowires, nanorods, and nanotubes have received a great deal of attention in the past decades. Their inherent anisotropic morphologies are able to overcome carbon corrosion issues that potentially lead to migration, aggregation, and Ostwald ripening of the isotropic 0 D Pt nanoparticles from the catalyst system.[36, 40-44]

Herein, we report a facile approach to synthesize unprecedented concave and duck web-like platinum nanopentagones (CWPNP) with a surface enclosed by {111} facets, high-energy {110} and {554} facets, multiple twin boundaries, duck-web like edges and inherent anisotropic branches. Such unique nanostructures exhibited remarkable enhanced electrocatalytic activities and durabilities for FOR.

2. Experimental section

2.1 Materials

Tri-n-propylamine, ethylenediamine, n-butylamine and tributylamine were purchased from Sinopharm Chemical Reagent Co.Ltd. (Shanghai, China). $Pt(acac)_2$ (acac=aceylacetonate) was bought from Alfa Aesar. H_2PtCl_6 was obtained from Shaanxi Kaida Chemical Engineering Co.Ltd. (China). Oleylamine, Nafion (10%), commercial Pt black (fuel cell grade, ≥99.9% trace metals basis) and Pd/C (30 wt. % loading) were purchased from Sigma-Aldrich. Commercial state-of-the-art 40 wt% Pt/C was obtained from Johnson Matthey Company**.** All chemicals were analytical-reagent grade and used without further purification. Teflon-lined autoclaves utilized in the synthetic protocol were

cleaned in a bath of freshly prepared 3 : 1 HCl : HNO_3 (aqua regia) and rinsed thoroughly in water prior to use. (CAUTION: aqua regia is highly corrosive and toxic; it should be handled with great care.)

2.2 Instrumentation

Scanning electron microscopy (SEM) images were recorded in a FEI XL30 ESEM FEG Scanning Electron Microscope operated at 25 kV. TEM images were all obtained using a FEI Tecnai G2 F20 microscope operated at 200 kV. Energy dispersive spectrometer (EDS) spectrums were collected in a Hitachi S-4800 Scanning Electron Microscope operated at 20.9 KV. X-ray diffraction (XRD) patterns were recorded on a Bruker D8 ADVANCE X-ray diffractometer (Cu Kα radiation) in the 30 to 80º 2theta range. The Fourier-transform infrared spectroscopy (FT-IR) spectra were recorded from KBr disks using a Perkin-Elmer GX instrument in the wavenumber range of 4000-400 cm^{-1}. Electrochemical experiments were performed in a CHI 660C electrochemistry workstation (Shanghai CHI Instruments Company, China) using modified glassy carbon working electrodes (ϕ = 3 mm), an Ag/AgCl reference electrode (saturated KCl), and a platinum wire counter electrode.

2.3 Preparation of Pt CWPNP

In a typical synthesis, 5 mg of $Pt(acac)_2$ was added to a mixed solution containing 4 mL of OAm and 4 mL of tri-n-propylamine. After ultrasonicating for around 30 minutes, the resultant homogeneous solution was transferred into a 20 mL Teflon-lined autoclave. The autoclave was maintained at 170 °C for 12 h and then cooled down to room temperature. The resulting black colloidal solutions were collected by centrifugation at 12000 rpm for 10 min, and washed with isopropanol and hexane several times. Final materials were redispersed in hexane.

2.4 Preparation of Pt/Pd catalysts modified electrodes

Pt CWPNP were treated with 99.5% acetic acid at 70 °C for overnight prior to modification to remove the remaining surfactant. The catalyst was separated by centrifugation and washed with water for two times.[45] The Pt/Pd catalysts were then resuspended in a mixture containing water, isopropanol, and Nafion (10%) (v:v:v 4:1:0.05) to form a 0.5 mg/mL catalyst ink. 2 µL catalyst inks were deposited on the glassy carbon working electrode that was polished prior to catalyst deposition by 0.3 µm and 0.05 µm alumina powders and rinsed by sonication in ethanol and in deionized water. The final Pt/Pd catalysts modified electrode was then dried at ambient condition prior to its use in the electrochemical reaction.

2.5 Electrochemical measurements

The test solutions were 0.5 M H_2SO_4, 0.5 M H_2SO_4 + 0.5 M formic acid. In the CV measurements, the electrode potential was scanned in the range of 0-0.9 V versus Ag/AgCl. Chronoamperometry was carried out at the constant potential of 0.28 V in 0.5 M H_2SO_4 + 0.5 M formic acid. All the catalyst electrodes were cleaned before datum collection with a CV in the range of -0.25-1.0 V versus Ag/AgCl at 50 mV/s. For the long-term stability test, accelerated cycling tests were also conducted up to 3000 cycles.

3. Results and discussion

In a typical synthesis of Pt CWPNP, $Pt(acac)_2$ was dissolved in a mixture of oleylamine and a common electrochemiluminescent co-reactant (tri-*n*-propylamine). After ultrasonicating for ca. 30 minutes, the resultant homogeneous solution was then solvothermally treated in a Teflon-lined stainless steel autoclave (20 mL in capacity) at 170 °C for 12 h. As the reaction proceeded, the solution color changed to black as depicted in Figure S1.

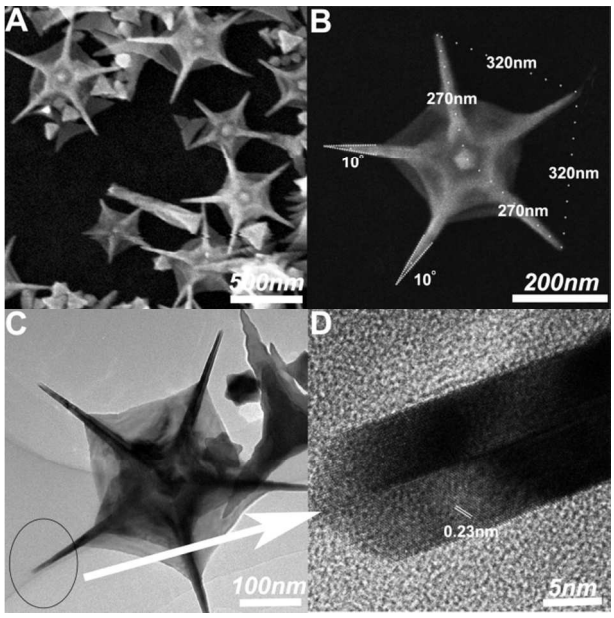

Fig. 1 (A) Large-area FESEM images and (B) enlarged FESEM images; C, D) TEM and HRTEM images of Pt CWPNP. Synthetic solution: 4 mL of oleylamine and 4 mL of tri-*n*-propylamine containing 5 mg of platinum (II) acetylacetonate.

Figure 1A shows a representative Field-Emission Scanning Electron Microscopy (FESEM) image of Pt CWPNP with an average size of ca. 540 nm. Over 60% of synthesized Pt nanoparticles are Pt CWPNP (Figure S2). Some icosahedra, tripods, rod-like particles and octapod Pt nanocrystals also co-existed with Pt CWPNP (Figure 1 and S3). The higher magnification FESEM image clearly depict Pt CWPNP features which include a five-fold twinned pentagonal nanoframe interior with concave surfaces, an exterior duck-web like contribution, and symmetric star-like branches. The distance between each of the adjacent apices is approximately equal (320 nm), and the distance from the center to each apex is approximately 270 nm. Each branch has a diameter of ca. 15 nm and a length of about 200 nm. The branches grow radially from a central core in five directions, thus suggesting that five-fold symmetric branches result from five-fold symmetric growth.

The morphology and structure of Pt CWPNP has been further characterized by Transmission Electron Microscopy (TEM) (Figure 1C). TEM images show a white contrast in the nanoframe section as compared to the edges/center regions. These findings indicate clear features of surface curving-in. The SAED pattern (Figure S4B) further displays the fivefold symmetry of the fcc structure spots, which is similar to the SAED pattern obtained on star-shaped Pt nanoparticles.[46] To better understand the crystalline characteristics of Pt CWPNP, high-resolution TEM

(HRTEM) measurements of a single branch tip were subsequently performed (Figure 1D). The branches are highly crystalline. The visible lattice fringes correspond to a space of 0.23 nm which matches well with the expected d spacing of (111) plane of Pt (0.226 nm). The HRTEM image also clearly shows the twinning boundaries. These above results prove firmly the five-fold twinning boundaries. Each tip's interfacial angle is about 10°. On the basis of the geometric shape of Pt CWPNP, the branch surface of Pt CWPNP seems to be bounded with {554} facets.[47] The crystalline nature of the obtained Pt duck-web like edges was also analyzed in depth. As shown in Figure S5, the majority of displayed facets showed lattice fringes with an interplanar spacing of 0.14 nm, corresponding to (110) planes of fcc Pt nanostructures. Furthermore, we performed Fast Fourier Transform (FFT) on the HRTEM image of the duck-web like edge of the nanocrystals and obtained patterns in accordance to electron diffraction patterns along the [011] zone axis, which supports the claim that duck-web like edges are enclosed by (110) facets. Energy dispersive X-ray (EDX) spectrum confirms the exclusive presence of Pt in as-prepared samples. Other contributions in EDX arise from ITO glass (Figure S6). X-ray diffraction (XRD) analyses further support the fact that the as-prepared samples exclusively consist of Pt in a face centered cubic structure (Pt JCPDS no.04-0802) (Figure S7).

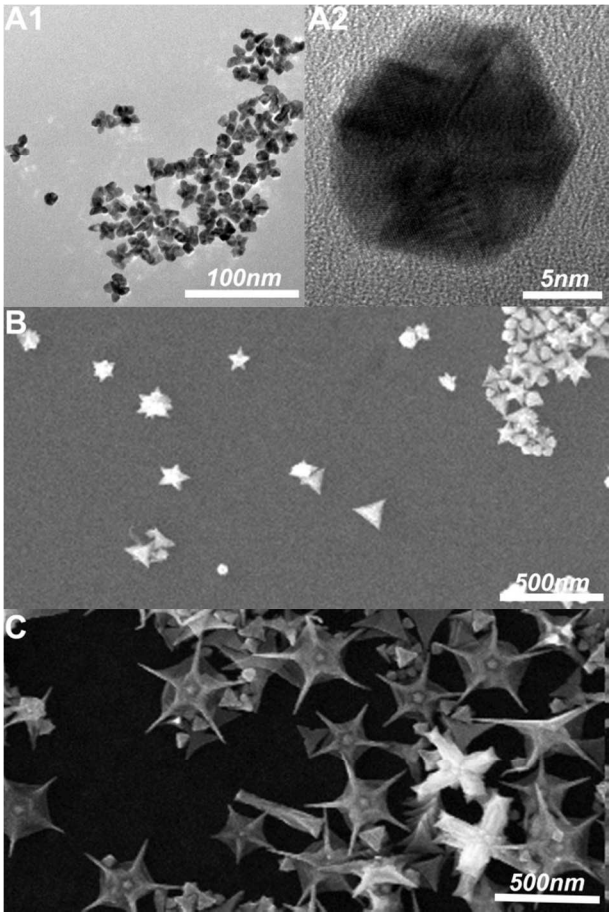

Fig. 2 FESEM and TEM images of Pt nanostructures collected at different growth stages. (A) 2, (B) 6, (C) 12 h. Synthetic solution: 4 mL of oleylamine and 4 mL of tri-*n*-propylamine containing 5 mg of platinum (II) acetylacetonate.

To further investigate the influencing factors in Pt CWPNP formation, some contrast experiments were also conducted. The morphological evolution of Pt nanocrystals at different reaction times was investigated by FESEM and HRTEM (Figure 2). Pt nanocrystals with sizes of ca. 20 nm, including many 5-fold twinned particles, are obtained after two hours of synthesis (Figure 2A). Upon increasing the time of reaction (from two hours to six hours), some star-shaped nanostructures are clearly observed (Figure 2B). Pt CWPNP is formed at longer times of reaction (typically 12 h, Figure 2C) from a fivefold twinned particle. Since the inhibition of oxidative etching of the twin defects by the exclusion of chloride ions has been reported to favor the generation of twinned nanostructures.[48] We also investigated the effect of the type of precursor on the morphology of as-synthesized Pt nanostructures. Irregular Pt nanocrystals were obtained if $Pt(acac)_2$ was replaced with H_2PtCl_6, indicating that the inhibition of oxidative etching is important for the formation of Pt CWPNP (Figure S8).[15]

Variations in content of tri-*n*-propylamine and oleylamine were also found to have a significant effect on the shape of synthesized nanostructures (Figure S9-S11). In the absence of tri-n-propylamine, only the irregular Pt nanoparticles were observed (Figure S9). A further increase of tri-*n*-propylamine concentration (25%) leads to a preferential formation of multipods with long branches (Figure S10A). Interestingly, Pt CWPNP is observed (Figure 2C) with an increase in the volume fraction of tri-n-propylamine to 50 %. The addition of tri-n-propylamine (up to 75%) results in the formation of Pt multipods with short branches in the product (Figure S10B). These results suggest that tri-*n*-propylamine is the major reason for the formation of braches enclosed by high-energy facets, due to the fact that amines can stabilize high index Pt facets.[49, 50] Nonetheless, a proper tri-*n*-propylamine/oleylamine ratio favors the nucleation of penta-twinned seeds, which direct the growth of five branches along the five twin boundary of the penta-twinned seeds. Oleylamine may play an important role in inhibiting the aggregation of metal nanoparticles.[51] So, irregular spherical aggregates are obtained with an increase in the volume fraction of tri-n-propylamine to 100 % (in the absence of oleylamine) (Figure S10C). To better understand the role of tri-*n*-propylamine in the formation of Pt CWPNP, the influence of some other organic amines on the synthesis of Pt nanostructures has been studied. Surprisingly, Pt CWPNP is not obtained by replacing tri-*n*-propylamine with other organic amines including ethylenediamine, *n*-butylamine and tributylamine (Figure S11). These results indicate that the addition of tri-*n*-propylamine is critical in the formation of Pt CWPNP. A comparison of the FT-IR spectra of the purified Pt CWPNP, tri-*n*-propylamine, and oleylamine shows the adsorption of oleylamine and tri-*n*-propylamine on the surfaces of purified Pt CWPNP (Figure S12). In the light of these premises, we believe that the different growth behaviors are most likely induced by the different chemisorptions properties and reducing capacities of oleylamine and tri-*n*-propylamine.

As-synthesized Pt CWPNPs are ideal model particles to investigate whether high FOR properties can be achieved. The electrocatalytic activity of Pt CWPNP was subsequently compared to that of commercial Pt black, Pt/C and Pd/C for FOR (Figure 3). The specific peak current density (Js) was normalized

to the electrochemically active surface area (ECSA). ECSA of the Pt catalysts was calculated from hydrogen adsorption/desorption charges of cyclic voltammograms in 0.5 M H_2SO_4 solutions (Figure S13) assuming 210 μC/cm^2. The reduction charge of the $Pd(OH)_2$ was employed to estimate ECSA values for the Pd catalysts based on the charge density (430 μC/cm^2) for the formation of a $Pd(OH)_2$ monolayer. Pt CWPNP exhibits three hydrogen desorption peaks at about –0.09 V, 0.05 V and 0.25 V, respectively. These peaks are consistent with the presence of {111}, {110} and {554} facets.[52] Js of FOR in the positive potential scan were 5.63 mA/cm^2 for Pt CWPNP. This value is 2.2, 8.5, and 27 times higher than that of commercial Pd/C, Pt/C and Pt black, respectively (Table S1). Pt CWPNP also possessed a lower potential for FOR at the same oxidation current density (Figure 3A). Furthermore, the specific activity of Pt CWPNP compares favorably with other recently reported highly performed catalysts (Table S2). The mass peak current density (Jm) of Pt CWPNP is 739 mA/mg, being 1.7, 6.8, and 23 times higher than that of commercial Pd/C, Pt/C and Pt black, respectively. The ratio of the first to the second peak current can give an indication of the main reaction path. The ratios of Pt CWPNP (1.49) are much higher as compared to those of commercial Pt/C (0.33) and Pt black (0.12). These findings suggest that Pt CWPNP can significantly promote the dehydrogenation path and decrease catalyst poisoning.[53] In addition, the first peak potential of Pt CWPNP was determined to be 0.28V, being 91 mV and 100 mV lower than that of Pt/C and Pt black, respectively. The improvement in current density, the first peak potential and antipoisoning activity of Pt CWPNP relates to their unique nanostructures. Firstly, high-energy facets and multiple twinned nanostructures have a large concentration of active sites especially important to break chemical bonds in electrocatalytic reactions. Secondly, Pt CWPNP with {111} surface coverage is least poisoned surfaces which can promote the dehydrogenation path. Last but not least, the duck web-like nanodomains may expose specific crystal planes therefore contributing to the observed remarkably enhanced electrocatalytic properties.[54-56]

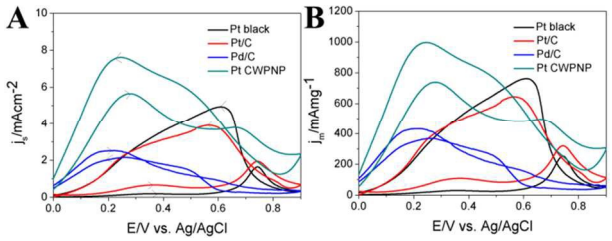

Fig. 3 Electrocatalytic activity of Pt CWPNP. Cyclic voltammograms of 0.5 M H_2SO_4 containing 0.5 M formic acid at Pt black, Pt/C, Pd/C and Pt CWPNP-modified glassy carbon electrode. Scan rate, 50 mV/s.

The electrochemical stability of the Pt black, Pt/C, Pd/C and Pt CWPNP electrocatalyst for FOR was further investigated by chronoamperometric experiments at a given potential of 0.28 V for 2000 s. Figure 4 summarizes typical current (i) – time (t) test results on various catalysts. Pt CWPNP exhibit improved stability as compared to commercial Pd/C, Pt/C and Pt black, during the 2000s i-t test (Figure 4A). The residual current densities (J_{2000s}) followed the order Pt CWPNP (1.62 mA/cm^2) > Pt/C (0.14 mA/cm^2) > Pd/C (0.12 mA/cm^2) > commercial Pt black (0.02 mA/cm^2) after 2000 s (Table S1). During the 2000 s test, the normalized Js (%) of Pt CWPNP (32), Pt/C (27) and commercial Pt black (11) also show remarkable differences (Figure 4B). The durability of these Pt catalysts was subsequently investigated by accelerated durability tests. As shown in Figure S14, the normalized Js (%) after 3000 cycles followed the order Pt CWPNP (74 %) > Pt/C (54 %) > Pt black (22 %) > Pd/C (6 %) in formic acid solution. SEM analysis further confirmed the stability of Pt CWPNP which generally remains almost unchanged after the FOR stability test (Figure S15). The enhanced stability of Pt CWPNP may be attributed to the unique anisotropic branched nanostructures composed of 1D nanowires which essentially make Pt less vulnerable to dissolution, migration, Ostwald ripening and aggregation. To demonstrate the potential of the Pt CWPNP catalyst in a direct formic acid fuel cell, the catalyst was integrated as the anode of a homemade fuel cell. The steady-state polarization and power-density curves of several catalysts were compared (Figure 5 A, B). The power density is 277 mW/cm^2 for Pt CWPNP. This value is 1.6 and 3.1 times higher than that of commercial Pd/C and Pt/C, respectively. Moreover, the Pt CWPNP catalyst also shows the most stable discharge ability at 0.35 V (Figure 5 C). These results demonstrate that Pt CWPNP is promising catalyst of direct formic acid fuel cell.

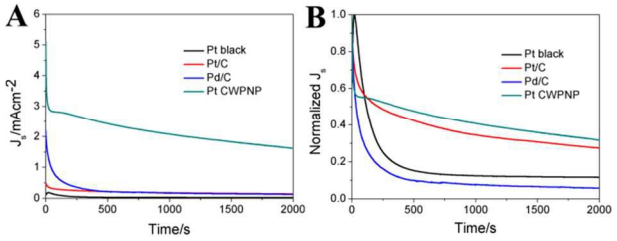

Fig. 4 Electrocatalytic stability of Pt CWPNP. (A) i-t curve of 0.5 M H_2SO_4 containing 0.5 M formic acid with Pt black, Pt/C, Pd/C and Pt CWPNP-modified glassy carbon electrodes. (B) Normalized j_s-time curve of 0.5 M H_2SO_4 containing 0.5 M formic acid with Pt black, Pt/C, Pd/C and Pt CWPNP-modified glassy carbon electrodes. I-t curves were collected at a constant potential of 0.28 V. The j_s are normalized with maximum current densities of each curve.

Conclusions

In conclusion, Pt CWPNP nanostructures have been reported for the first time and exploited it as a novel electrocatalyst for FOR. The synthesized Pt CWPNP exhibits remarkable performances towards FOR in comparison to commercial catalysts. The outstanding electrocatalytic performance can be ascribed to following three reasons: 1) The least poisoned {111} facets can enhance poisoning resistance; 2) The active sites by high-energy facets, multiple twin boundaries can enhance electrocatalytic activity; 3) The inherent anisotropic branches composed of 1D nanowires can enhance electrocatalytic stability. Such unique nanostructures may pave the way to new perspectives for fundamental research on advanced surface structure-controlled electrocatalysts for electrocatalysis.

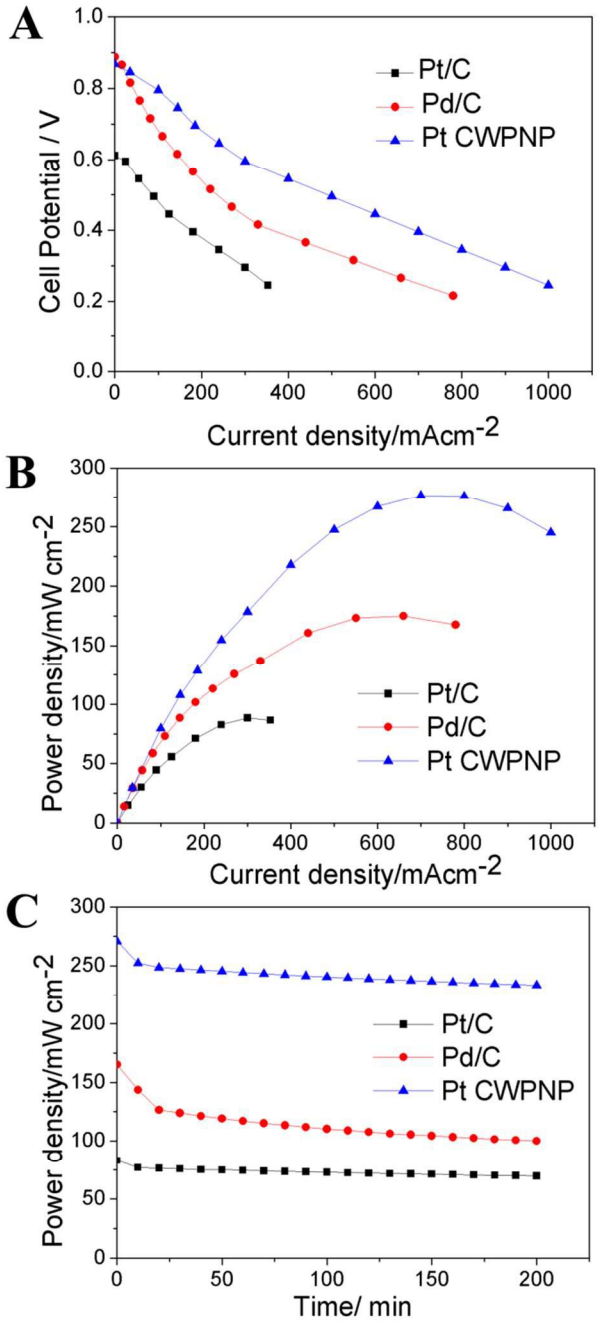

Fig. 5 (A) Steady-state polarization, (B) power density curves, and (C) discharge curves at 0.35 V for the direct formic acid fuel cell containing membrane electrode assemblied with Pt/C, Pd/C and Pt CWPNP as anode catalysts, a Nafion 117 membrane, and Pt/C (40wt%, Johnson Metthey) cathode catalysts at 30 °C. The flow rate of formic acid (3 M) was 200 mL min^{-1} and the flow rate of O_2 was 500 mL min^{-1}.

Acknowledgements

This project was supported by the National Natural Science Foundation of China (No. 21175126) and Chinese Academy of Sciences Visiting Professorships for Senior International Scientists (No. 2013T2G0024).

Notes and references

[a] *State Key Laboratory of Electroanalytical Chemistry, Changchun Institute of Applied Chemistry, Chinese Academy of Sciences, 5625 Renmin Street, Changchun 130022, China. Fax: +86-431-85262747, Tel: +86-431-85262747, E-mail: guobaoxu@ciac.ac.cn;*
[b] *University of the Chinese Academy of Sciences, Chinese Academy of Sciences, No. 19A Yuquanlu, Beijing 100049, China;*
[c] *Departamento de Química Orgánica, Universidad de Córdoba Campus de Rabanales, Edificio Marie Curie (C-3), Ctra Nnal IV, Km 396, Córdoba (Spain), E-14014, E-mail: q62alsor@uco.es.*

† Electronic Supplementary Information (ESI) available: [details of any supplementary information available should be included here]. See DOI: 10.1039/b000000x/

1. R. F. Service, *Science*, 2002, **296**, 1222-1224.
2. E. Casado-Rivera, D. J. Volpe, L. Alden, C. Lind, C. Downie, T. Vázquez-Alvarez, A. C. D. Angelo, F. J. DiSalvo and H. D. Abruña, *J. Am. Chem. Soc.*, 2004, **126**, 4043-4049.
3. Y. X. Chen, M. Heinen, Z. Jusys and R. J. Behm, *Angew. Chem. Int. Ed.*, 2006, **45**, 981-985.
4. J. Solla-Gullon, F. J. Vidal-Iglesias, A. Lopez-Cudero, E. Garnier, J. M. Feliu and A. Aldaz, *Phys. Chem. Chem. Phys.*, 2008, **10**, 3689-3698.
5. H. Abe, F. Matsumoto, L. R. Alden, S. C. Warren, H. D. Abruña and F. J. DiSalvo, *J. Am. Chem. Soc.*, 2008, **130**, 5452-5458.
6. S. Uhm, H. J. Lee, Y. Kwon and J. Lee, *Angew. Chem. Int. Ed.*, 2008, **47**, 10163-10166.
7. X. Ji, K. T. Lee, R. Holden, L. Zhang, J. Zhang, G. A. Botton, M. Couillard and L. F. Nazar, *Nat. Chem.*, 2010, **2**, 286-293.
8. D. Xu, S. Bliznakov, Z. Liu, J. Fang and N. Dimitrov, *Angew. Chem. Int. Ed.*, 2010, **49**, 1282-1285.
9. F. J. Vidal-Iglesias, J. Solla-Gullón, E. Herrero, A. Aldaz and J. M. Feliu, *Angew. Chem. Int. Ed.*, 2010, **49**, 6998-7001.
10. S. Zhang, Y. Shao, G. Yin and Y. Lin, *Angew. Chem. Int. Ed.*, 2010, **49**, 2211-2214.
11. M. Osawa, K.-i. Komatsu, G. Samjeské, T. Uchida, T. Ikeshoji, A. Cuesta and C. Gutiérrez, *Angew. Chem. Int. Ed.*, 2011, **50**, 1159-1163.
12. X. Chen, G. Wu, J. Chen, X. Chen, Z. Xie and X. Wang, *J. Am. Chem. Soc.*, 2011, **133**, 3693-3695.
13. W. Gao, J. E. Mueller, Q. Jiang and T. Jacob, *Angew. Chem. Int. Ed.*, 2012, **51**, 9448-9452.
14. M. K. Debe, *Nature*, 2012, **486**, 43-51.
15. L. Ma, C. Wang, M. Gong, L. Liao, R. Long, J. Wang, D. Wu, W. Zhong, M. J. Kim, Y. Chen, Y. Xie and Y. Xiong, *ACS Nano*, 2012, **6**, 9797-9806.
16. M. Jin, H. Zhang, Z. Xie and Y. Xia, *Energy Environ. Sci.*, 2012, **5**, 6352-6357.
17. S. Zhang, S. Guo, H. Zhu, D. Su and S. Sun, *J. Am. Chem. Soc.*, 2012, **134**, 5060-5063.
18. F. J. Vidal-Iglesias, A. López-Cudero, J. Solla-Gullón and J. M. Feliu, *Angew. Chem. Int. Ed.*, 2013, **52**, 964-967.
19. J. Joo, T. Uchida, A. Cuesta, M. T. M. Koper and M. Osawa, *J. Am. Chem. Soc.*, 2013, **135**, 9991-9994.
20. X. Wang, J. Yang, H. Yin, R. Song and Z. Tang, *Adv. Mater.*, 2013, **25**, 2728-2732.
21. J. Chang, L. Feng, C. Liu, W. Xing and X. Hu, *Angew. Chem. Int. Ed.*, 2014, **53**, 122-126.
22. K. Jiang, H.-X. Zhang, S. Zou and W.-B. Cai, *Phys. Chem. Chem. Phys.*, 2014, **16**, 20360-20376.

23. T. Y. Ma, J. Ran, S. Dai, M. Jaroniec and S. Z. Qiao, *Angew. Chem. Int. Ed.*, 2014, **54**, 4646-4650.
24. J. Lai, W. Niu, R. Luque and G. Xu, *Nano Today*, 2015, **10**, 240-267.
25. M. E. Scofield, C. Koenigsmann, L. Wang, H. Liu and S. S. Wong, *Energy Environ. Sci.*, 2015, **8**, 350-363.
26. Y. Jiao, Y. Zheng, M. Jaroniec and S. Z. Qiao, *Chem. Soc. Rev.*, 2015, **44**, 2060-2086.
27. S. Chen, H. Su, Y. Wang, W. Wu and J. Zeng, *Angew. Chem. Int. Ed.*, 2014, **54**, 108-113.
28. J. Lai, R. Luque and G. Xu, *ChemCatChem*, 2015, **7**, 3206-3228.
29. J. Clavilier, *J. Electroanal. Chem.*, 1987, **236**, 87-94.
30. S. G. Sun, J. Clavilier and A. Bewick, *J. Electroanal. Chem.*, 1988, **240**, 147-159.
31. V. Grozovski, V. Climent, E. Herrero and J. M. Feliu, *Phys. Chem. Chem. Phys.*, 2010, **12**, 8822-8831.
32. J. Xu, D. Yuan, F. Yang, D. Mei, Z. Zhang and Y.-X. Chen, *Phys. Chem. Chem. Phys.*, 2013, **15**, 4367-4376.
33. N. Tian, Z.-Y. Zhou, S.-G. Sun, Y. Ding and Z. L. Wang, *Science*, 2007, **316**, 732-735.
34. L. Zhang, W. Niu and G. Xu, *Nano Today*, 2012, **7**, 586-605.
35. Z. Quan, Y. Wang and J. Fang, *Acc. Chem. Res.*, 2012, **46**, 191-202.
36. J. Lai, W. Niu, W. Qi, J. Zhao, S. Li, W. Gao, R. Luque and G. Xu, *ChemCatChem*, 2015, **7**, 1064-1069.
37. B. Y. Xia, H. B. Wu, X. Wang and X. W. Lou, *Angew. Chem. Int. Ed.*, 2013, **52**, 12337-12340.
38. A.-X. Yin, X.-Q. Min, W. Zhu, H.-S. Wu, Y.-W. Zhang and C.-H. Yan, *Chem. Commun.*, 2012, **48**, 543-545.
39. L. Ruan, E. Zhu, Y. Chen, Z. Lin, X. Huang, X. Duan and Y. Huang, *Angew. Chem. Int. Ed.*, 2013, **52**, 12577-12581.
40. Z. Chen, M. Waje, W. Li and Y. Yan, *Angew. Chem. Int. Ed.*, 2007, **46**, 4060-4063.
41. C. Koenigsmann and S. S. Wong, *Energy Environ. Sci.*, 2011, **4**, 1161-1176.
42. S. Guo, D. Li, H. Zhu, S. Zhang, N. M. Markovic, V. R. Stamenkovic and S. Sun, *Angew. Chem. Int. Ed.*, 2013, **52**, 3465-3468.
43. B. Y. Xia, H. B. Wu, Y. Yan, X. W. Lou and X. Wang, *J. Am. Chem. Soc.*, 2013, **135**, 9480-9485.
44. B. Y. Xia, W. T. Ng, H. B. Wu, X. Wang and X. W. Lou, *Angew. Chem. Int. Ed.*, 2012, **51**, 7213-7216.
45. V. Mazumder and S. Sun, *J. Am. Chem. Soc.*, 2009, **131**, 4588-4589.
46. L.-M. Lacroix, C. Gatel, R. Arenal, C. Garcia, S. Lachaize, T. Blon, B. Warot-Fonrose, E. Snoeck, B. Chaudret and G. Viau, *Angew. Chem. Int. Ed.*, 2012, **51**, 4690-4694.
47. H.-G. Liao, Y.-X. Jiang, Z.-Y. Zhou, S.-P. Chen and S.-G. Sun, *Angew. Chem. Int. Ed.*, 2008, **47**, 9100-9103.
48. H. Zhang, X. Xia, W. Li, J. Zeng, Y. Dai, D. Yang and Y. Xia, *Angew. Chem. Int. Ed.*, 2010, **49**, 5296-5300.
49. X. Huang, Z. Zhao, J. Fan, Y. Tan and N. Zheng, *J. Am. Chem. Soc.*, 2011, **133**, 4718-4721.
50. L. Zhang, D. Chen, Z. Jiang, J. Zhang, S. Xie, Q. Kuang, Z. Xie and L. Zheng, *Nano. Res.*, 2012, **5**, 181-189.
51. S. Mourdikoudis and L. M. Liz-Marzán, *Chem. Mater.*, 2013, **25**, 1465-1476.
52. J. Solla-Gullon, P. Rodriguez, E. Herrero, A. Aldaz and J. M. Feliu, *Phys. Chem. Chem. Phys.*, 2008, **10**, 1359-1373.
53. Z. Cui, M. Yang and F. J. DiSalvo, *ACS Nano*, 2014, **8**, 6106-6113.
54. F. Saleem, Z. Zhang, B. Xu, X. Xu, P. He and X. Wang, *J. Am. Chem. Soc.*, 2013, **135**, 18304-18307.
55. Y. Jia, Y. Jiang, J. Zhang, L. Zhang, Q. Chen, Z. Xie and L. Zheng, *J. Am. Chem. Soc.*, 2014, **136**, 3748-3751.
56. A. Funatsu, H. Tateishi, K. Hatakeyama, Y. Fukunaga, T. Taniguchi, M. Koinuma, H. Matsuura and Y. Matsumoto, *Chem. Commun.*, 2014, **50**, 8503-8506.